Contents lists available at GrowingScience

Current Chemistry Letters

homepage: www.GrowingScience.com

Synthesis, characterization and optical band gap of Pirochromite ($MgCr_2O_4$) Nanoparticles by Stearic Acid Sol-Gel Method

Ehsan Jafarnejad[a*], Salah Khanahmadzadeh[a], Fatemeh Ghanbary[a] and Morteza Enhessari[b]

[a]*Department of Chemistry, Mahabad Branch, Islamic Azad University, Mahabad, P.O. Box 443, Iran*
[b]*Department of Chemistry, Naragh Branch, Islamic Azad University, Naragh, Iran*

C H R O N I C L E

Article history:
Received January 21, 2016
Received in revised form
July 10, 2016
Accepted 11 July 2016
Available online
11 July 2016

Keywords:
Nanoparticles
Pirochromite
AB_2O_4
Sol-gel method
Fd_3m

A B S T R A C T

Pirochromite ($MgCr_2O_4$) nanoparticles were successfully prepared in this study. During synthesis of the pirochromite nanoparticles, a sol-gel was prepared by using magnesium acetate and potassium dichromate as magnesium and chromium sources and by using stearic acid as the network. Infrared spectroscopy (FT-IR), X-ray diffraction (XRD), transmission electron microscope (TEM), scanning electron microscope (SEM), and energy-dispersive X-ray spectroscopy (EDX) were used for the elemental analysis, and diffuse reflectance spectroscopy (DRS) and vibrating sample magnetometer (VSM) were used in order to identify, provide a fuzzy diagnosis, and determine the size and morphology of the particles, as well as to analyze the optical and magnetic properties of the particles. The particle size of $MgCr_2O_4$ nanoparticles was observed to fall within a range of 39 nm–71 nm.

1. Introduction

Nanoparticles have unique properties, such as high resistance, toughness, and rigidity, due to their high surface area to volume ratio. Magnesium oxide is a powder nanocompound; its spinel structure consists of a very large family of compounds with a wide range of physical properties, which has attracted great interest in the scientific community [1]. $MgCr_2O_4$ is traditionally created by a solid state reaction that requires a high temperature, which leads to a lower specific surface area and lower catalytic activity for the synthesized material, Synthesis and Characterization of Pirochromite ($MgCr_2O_4$) Nanoparticles by Stearic Acid Sol-Gel Method was successfully prepared in this study. Magnesium chromate spinel, MgCr2O4, is a well-known refractory material due to its high-melting point (2350°C), high chemical inertness against both acidic and basic slags, and high strength at elevated temperatures. MgCr2O4 is used in a wide range of industrial furnaces such as in secondary refining, non-ferrous metal metallurgy, cement rotary kilns, thermocouple protection tube, coal gasifier lining, glass furnace, etc. For its many applications, the nanosized spinel particles are greatly desired because nanocrystalline MgCr2O4 spinel particles certainly

* Corresponding author.
E-mail address: jafarnejade@yahoo.com (E. Jafarnejad)

doi: 10.5267/j.ccl.2016.7.001

offer higher sintering reactivity, consequently decrease the sintering temperature of the product, and improve the properties of the products. The spinel structure includes a large family of compounds that exhibit a wide variety of physicochemical properties with important practical applications [2]. Thus, spinel oxides (AB_2O_4), pirochromite ($MgCr_2O_4$), and other related binary oxides have important technological applications, including their use as magnetic materials, high-temperature ceramics [3], strengthening agents, sensor elements, interconnecting materials for solid oxide fuel cells, combustion catalysts, or catalytic supports [4-8]. For many of these applications, achievement of high surface area materials is greatly desired. The spinel $MgCr_2O_4$ displays a cubic structure belonging to the space group Fd_3m, in which Mg and Cr ions occupy the tetrahedral and octahedral sites, respectively. $MgCr_2O_4$ has been taken as a model transition metal oxide combustion catalyst for chromite-related materials. The catalytic activity of this material in the oxidation of propane and propene has been also investigated, confirming that $MgCr_2O_4$ is an efficient complete combustion catalyst [9-12]. Magnesium oxide is an insulating material that has a high heat transfer capacity, and its binary spinel ($MgCr_2O_4$) and the other relevant binary oxide (Fe, Co, Ni) have important applications in different technologies, such as magnetic materials, high-temperature ceramics, and reinforcing agents, and can be used as sensors or elements that are intelligent and combustion catalysts[13]. The spinel structure of $MgCr_2O_4$ represents a cubic structure belonging to the Fd_3m space group, in which magnesium and chromium ions are occupied in hexagonal and octagonal molecular shapes[14]. Although the metallurgical use of magnesium oxide is to provide resistance to decay and to create a brilliant shine as a component in alloys, such as stainless steel and chrome plating, and to serve as a catalyst in applications, $MgCr_2O_4$ is also used as a catalyst for the oxidation of propene and propane[15]. To overcome this limitation, in this study, nano-sized $MgCr_2O_4$was prepared by using a sol-gel synthesis process, as shown in Scheme 1.

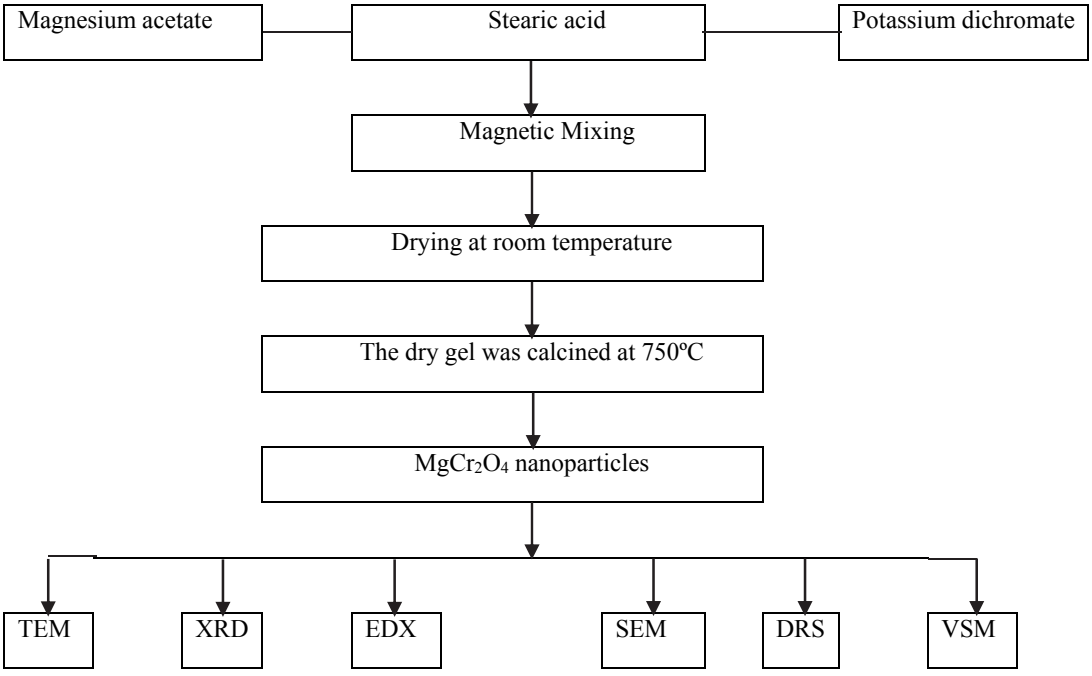

Scheme 1. Magnesium oxide nanoparticles preparing

2. Experiment

The chemical compounds that were employed in this work were obtained from Merck and were used with no purification. Transmission electron microscope (*TEM*) Scanning electron microscopy (SEM) analysis was performed on a Philips XL-30 field-emission scanning electron microscope operated at 16 kV. X-ray diffraction, XRD, and EDX were performed on the EM 3200model, manufactured by KYKY. The TEM pictures were recorded with Philips model EM 208 instrument at

the accelerating voltage of 100 kV. The fine powders were dispersed in amyl acetate on a carbon-coated TEM copper grid. SEM was equipped with a LEO1455 UP, Oxford, UK. The UV–vis diffused reflectance spectra (DRS) were obtained from UV–vis Scinco 4100 spectrometer with an integrating sphere reflectance accessory. BaSO4 was used as reference material; UV–vis absorption spectra were recorded using a Shimadzu 1600 PC in the spectral range of 190–900 nm.

2.1. Synthesis of the $MgCr_2O_4$ Nanoparticles

To synthesize the $MgCr_2O_4$ nanoparticles, stearic acid (0.4 mol) was melted in a beaker at 73°C. Magnesium acetate (0.1 mol) was then added to it. At this stage, a homogeneous solution was obtained. A potassium dichromate solution (0.2 mol) was added afterward and stirred until a homogeneous solution was obtained. This solution was cooled to room temperature and put in the oven for 6 hours to obtain a dry gel. Finally, the dry gel was calcined at 750°C; after it was cooled to room temperature for a few hours, $MgCr_2O_4$ nanoparticles were obtained[16].

3. Results and Discussion

3.1. XRD Pattern of the $MgCr_2O_4$ Composition

To determine the composition of the $MgCr_2O_4$ crystalline structure, the XRD pattern was recorded. As shown in Fig. 1, the XRD pattern of the composition is in agreement with the reference pattern. The sharp peaks observed at 18° (2θ) , 37° (2θ), and 43° (2θ) indicated the presence of Mg, Cr, and O. Additionally, the observed peaks at 56 ° (2θ) and 63° (2θ) are related to the formation of Cr_2O_3 and CrO, respectively. As expected, the highest degree of crystallite was achieved when the calcined temperature occurred in the synthesis process[17].

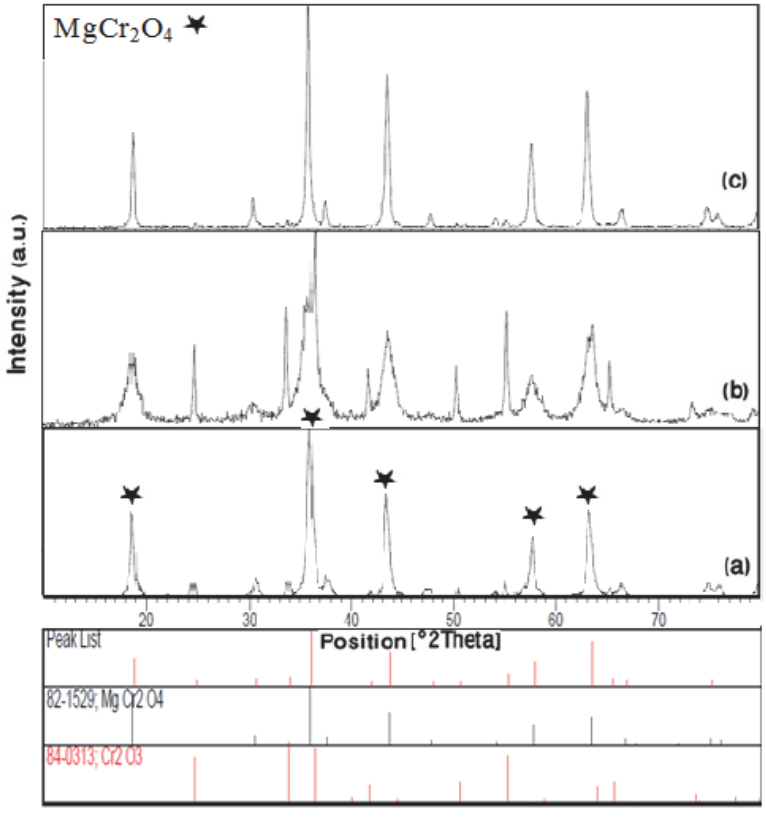

Fig. 1.The XRD Diffraction Patterns of the $MgCr_2O_4$ Composition Calcined at (a) 600°C; (b) 700°C and (c) 750°C

3.2. Morphology of samples

XRD has been performed on powder and the particle size L has been estimated with Scherrer formula (Eq. (1)) [18]:

$$L = \frac{K \times \lambda}{\Delta(2\theta) \times \cos(\theta)}, \quad (1)$$

where K is the form factor (equal to 0.9), $\lambda = 0.15418$ nm, 2θ the peak position and $\Delta(2\theta)$ the full width at half maximum of the diffraction peak in terms of radians. In this way, we find that the crystallite size of the powders Calcined at 600°C, 700°C and 750°C were about 39 nm. Figure 2(a) shows a typical bright-field TEM image of the $MgCr_2O_4$ nanoparticles from the solution. All $MgCr_2O_4$ nanoparticles have a narrow size distribution. The particles are in the size 39 nm to 71 nm, and the average size of particles obtained from two methods is close approximately. Figure 2(b) shows the morphologies of $MgCr_2O_4$ products by SEM. It indicated that the size of the particles was homogeneous.

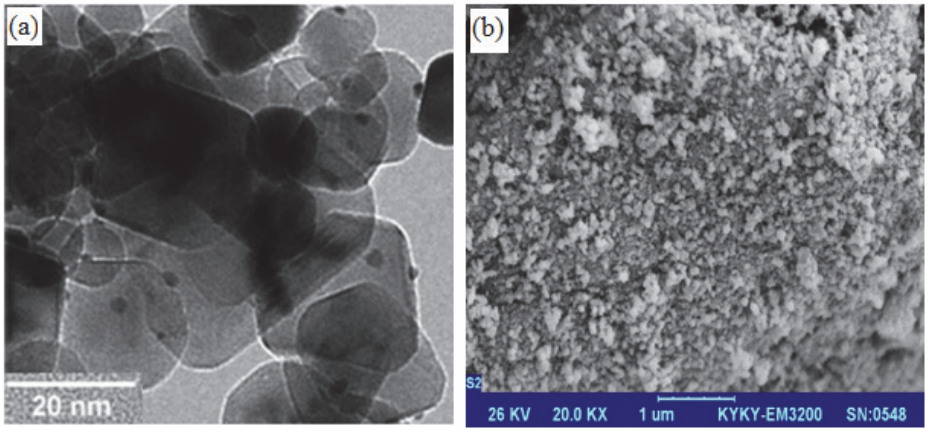

Fig. 2. (a) TEM (b) SEM pictures of $MgCr_2O_4$ Nanoparticles

3.3. EDX Elemental Analysis

This type of spectrum is obtained as a result of bombarding samples with X-rays, electrons, or protons to determine the elements .Fig. 3 shows the EDX pattern of the $MgCr_2O_4$ nanoparticles. The EDX analysis of the calcined nano-powder created in the 900°C and 750°C environment illustrated the presence of Mg, Cr, and O, which confirms the production of $MgCr_2O_4$.

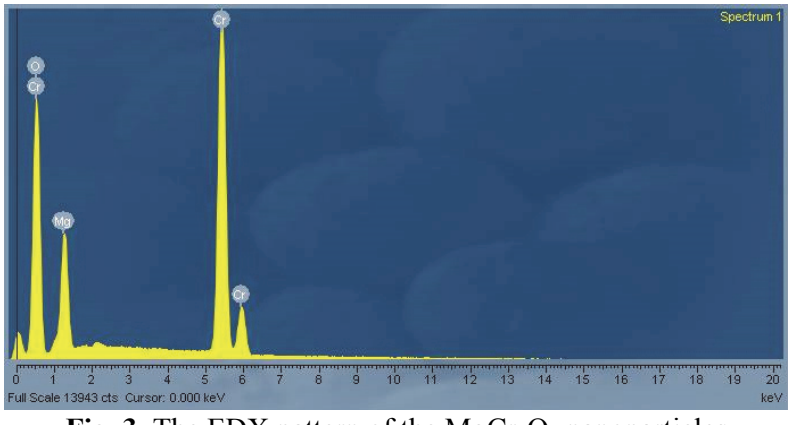

Fig. 3. The EDX pattern of the $MgCr_2O_4$ nanoparticles

3.4. DRS Analysis

The absorption coefficient and optical band gap of a material are two important parameters by which the optical characteristics and its practical applications in various fields are judged. Figure 4 shows the DRS of pure $MgCr_2O_4$. In Fig. 4, a sharp absorption peak is observed around 250 nm, indicating the optical band gap attributed to the Cr3+ to Cr2+ charge-transfer interaction XP spectra reveal that a fraction of chromium appears in the form of Cr6+ species. Taking into account that its reduction is relatively easy when it is present in unsupported chromium oxides, the first reduction step (below 750°C) can be assigned to the reduction of Cr6+ to Cr3+. Besides, the reduction of Cr3+ to Cr2+ can apparently take place in the region above 750°C. The system operates based on casting light on the material surface and measuring the amount of reflected light in comparison with a standard (non-absorption of the dispersion, usually $BaSO_4$). Measuring dispersive-reflection is particularly useful for evaluating the properties of powdered materials. The DRS chart of $MgCr_2O_4$ nanoparticles is shown in Figure 4, in which the maximum absorbance was apparent at 250 nm [19].

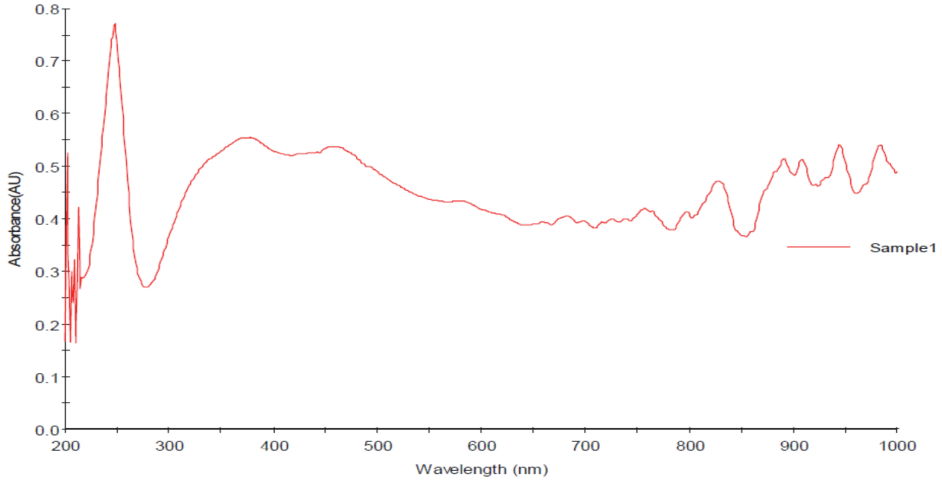

Fig. 4 .The DRS chart of $MgCr_2O_4$ nanoparticles

3.5. Band-GapAnalysis

For direct band gap determination, a plot of $(\alpha h\upsilon)^2$versus $h\upsilon$ is presented in Figure 5. Band gap value was obtained by extrapolating the straight portion of the graph on the hυaxis at $(\alpha h\upsilon)^2$=0, as indicated by the solid line in Fig. 5. Usually, the band-gap of the nanomaterials is larger than that of nano-crystallines or of non-nano materials. With an increase in the band-gap, the particle size of the semiconductor material decreases. The energy gap is an important feature of semiconductor materials, which determines their application abilities in optoelectronics[20]. Band-gap measurements are obtained through the absorption curve, in which α is a linear absorption coefficient of the matter. A semiconductor with a large band-gap cannot absorb a lot of light in solar cells. Thus, the use of synthesized salts on solar panels was introduced. Solar cells have material with a large band-gap. Synthesized salts are organic molecules that can absorb light on the surface of porous electrodes and that start the conversion of light to electrical current [21-22]. However, the use of a material with a large band-gap is not efficient enough for solar cells; two large band-gap materials are needed, as this current has to come to a nanowire. Fig. 5 shows the band-gap diagram of $MgCr_2O_4$ nanoparticles at a rate of approximately 1.8 eV, while the value in the $MgCr_2O_4$ bulk is 1.3 eV. This increase in the value of the band-gap indicates that the material has gained semiconductor properties[23].

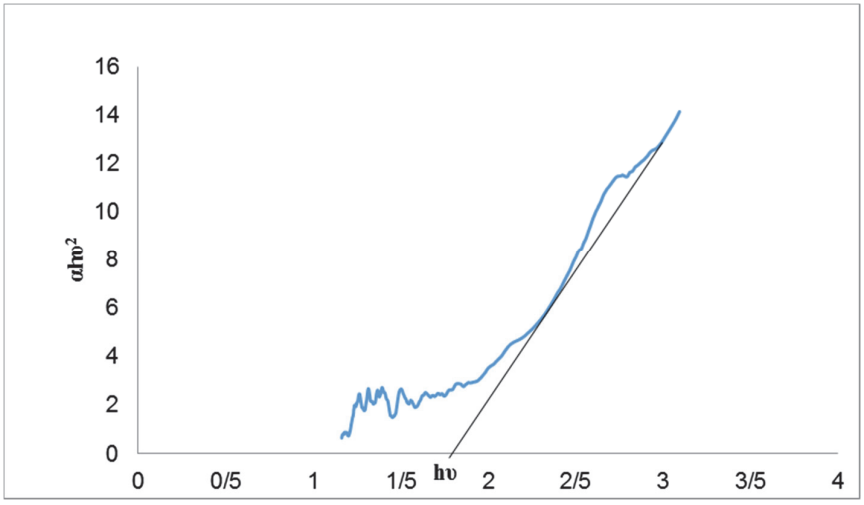

Fig. 5. The band-gap diagram of $MgCr_2O_4$ nanoparticles

3.6. Vibrating Sample Magnetometer Micrograph

Fig. 6 shows the vibrating sample magnetometer micrograph of the $MgCr_2O_4$ nanoparticles. As the figure indicates, $MgCr_2O_4$ nanoparticles are paramagnetic. Their magnet value is approximately 0.2 emu g^{-1}.

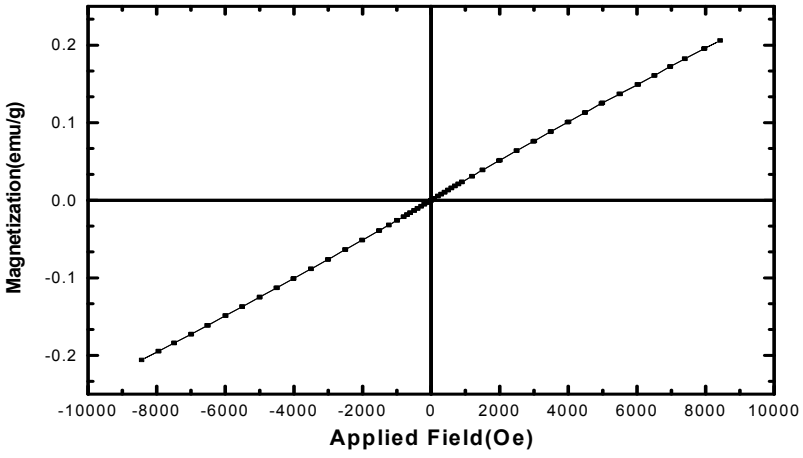

Fig. 6. The vibrating sample magnetometer micrograph of the $MgCr_2O_4$ nanoparticles

4. Conclusions

This paper investigated the synthesis and characterization of $MgCr_2O_4$ nanoparticles. The results obtained from the use of FT-IR, DRS, SEM, EDX, XRD, and VSM, and the subsequent comparison with reference patterns indicated that the preparation process of the nanoparticles in this study is appropriate. The particle size of the synthesized $MgCr_2O_4$ was in the range of 39 nm to 71 nm. The band-gap of the $MgCr_2O_4$ nanoparticles was also obtained and showed the rate of approximately 1.8 eV. Additionally, the VSM results indicated that the $MgCr_2O_4$ nanoparticles are paramagnetic. Their magnet value was approximately 0.2 emu g^{-1}. Although the metallurgical use of magnesium oxide is to provide resistance to decay and to create a brilliant shine as a component in alloys, such as stainless steel and chrome plating,

and to serve as a catalyst in applications, $MgCr_2O_4$ is also used as a catalyst for the oxidation of propene and propane.

Acknowledgements

The authors gratefully acknowledge Mahabad branch, Islamic Azad University and Iranian Nanotechnology Initiative for providing financial support and encouragement.

References

1. Hailiang L., Wenling M., Hongxia Z., Jiyong D., Xiaohua, Y. (**2011**) Synthesis and Characterization of $MgCr_2O_4$:Co^{2+} Fabricated by a Microwave. *Mater Manuf. Process*., 2 (6) 1-5
2. Enhessari, M. (**2013**) Synthesis, characterisation and optical band gap of $Cr_{1.3}Fe_{0.7}O_3$ nanopigments. *Pigment & Resin Technology*, 42 (6) 347-352.
3. Manoharana S. S., Patil K. S. (**1992**) Photoluminescent properties of Mg doped ZnO by microwave combustion and microwave polyol method. *J. Am. Ceram. Soc*., 1 (5) 10-12.
4. Yuvaraj S.V., Nithya D. K., Saiadali F., Sanjeeviraja G., Kalai S. (**2013**) Investigations on the temperature dependent electrical and magnetic, properties of NiTiO3 by molten saltsynthesis. *Mater. Res. Bull.,* 4 (8) 1110–1116.
5. Kesler, V. G. (**2003**) Molecular structure design and synthetic approaches to the heterometallic alkoxide complexes. *Chem. Commun.,* 1 (4) 1213–1222.
6. Pouillerie C., Croguennec L., Biensan Ph., Willmann P., Delmas C. (**2000**) Synthesis and Characterization of New $LiNi_{1-y}Mg_yO_2$ Positive Electrode Materials for Lithium-Ion Batteries. *J. Electrochem. Soc*., 4 (7) 20-61.
7. Martinho H., Moreno N. O., Sanjurjo J. A., Rettori C., García-Adeva A. J., Huber D. L., Oseroff S. B., Ratcliff W., II, Cheong S.-W., Pagliuso P. G., Sarrao J. L., Martins G. B. (**2001**) Magnetic properties of the frustrated antiferromagnetic spinel $ZnCr_2O_4$ and the spin-glass $Zn_{1-x}Cd_xCr_2O_4$ (x=0.05,0.10). *Phys. Rev. B*., 6 (4) 21–61.
8. Kim B.N., Hiraga K. Morita K., Sakka, Y. (**2001**) A high-strain-rate superplastic ceramic. *Nature*, 4 (13) 288-291.
9. Hashimoto S., Yamagushi A. (**1995**) Growth and characterization of needle-like β-$CaCr_2O_4$ crystals. *J. Cryst. Growth*, 1 (5) 29-43.
10. Segal D. (**1997**) Chemical synthesis of ceramic materials. *J. Mater. Chem*., 7 (7) 1297–1305.
11. Drazic G., Trontel M. (**1989**) Preparation and properties of ceramic sensor elements based on $MgCr_2O_4$. *J. Sens. Actuators*, 1 (8) 40-71.
12. Pingale S. S., Patil S. F., Vinod M. P., Pathak G. (**1996**) Mechanism of humidity sensing of Ti-doped $MgCr_2O_4$ ceramics. *Mater. Chem. Phys*., 4 (6) 72-78.
13. Lee A. N., Hwang A. I. S., Yoo, H. I. (**2001**) Nanocrystalline pirochromite spinel through solution combustion synthesis. *Nucl. Eng. Des*., 2 (5) 5- 23.
14. Nitta T., Terada Z., Hayakawa, S. (**1980**) .Humidity-Sensitive Electrical Conduction of $MgCr_2O_4$-TiO_2 Porous Ceramics. *J. Am. Ceram. Soc*., 6 (3) 29-51.
15. Schoonman J., Dekker J. P., Broers, J. W. (**1991**) Electrochemical vapor deposition of stabilized zirconia and interconnection materials for solid oxide fuel cells. *Solid State Ionics*, 4 (6) 299-301.
16. Finocchio E., Busca G., Lorenzelli V., Willey, R. J. (**1995**) The Activation of Hydrocarbon C-H Bonds over Transition Metal Oxide Catalysts: A FTIR Study of Hydrocarbon Catalytic Combustion over $MgCr_2O_4$. *J. Catal*., 1 (51) 20-41.
17. Busca G., Daturi M., Finocchio E., Lorenzelli V., Ramis, G. (**1997**) Transition metal mixed oxides as combustion catalysts: preparation, characterization and activity mechanisms. *Catal. Today*, 3 (3) 2-39.
18. Finocchio E., Ramis G., Busca G., Lorenzelli V., Willey R. J. (**1996**) On the mechanisms of light alkane catalytic oxidation and oxy-dehydrogenation: an FT-IR study of the n-butane conversion over $MgCr_2O_4$ and a Mg-vanadate catalyst. *Catal. Today*, 2 (8) 3-81.

19. Jafarnejad E., Sonia R., Ghanbarizadeh M. (**2016**) Synthesis and Characterization Nanocomposite of the Graphene Oxide/Polyacrylic acid Modified with 2-Mercaptoethanol. *Polymer Science, Series B*, 58 (3) 366–370.
20. Enhessari M., Parviz A., Ozaee K., Karamali E. (**2010**) Magnetic properties and heat capacity of CoTiO3 nanopowders prepared by stearic acid gel method. *J. Exp. Nanosci*., 1 (5) 61–68.
21. Nagata K., Nishiwaki R., Nakamura Y., Maruyama T. (**1991**) Kinetic mechanisms of the formations of MgCr2O4 and FeCr2O4 spinels from their metal oxides. *Solid State Ionics*, 4 (9) 1-61.
22. Hesse, D. (**1997**) Control of phase formation and film orientation by molar volume stress during MgO-GeO_2 thin-film solid-solid reactions. *Solid State Ionics*, 9 (5) 11-51.
23. Zhang N. M., Teraoka Y., Yamazoe N. (**1987**) Oxidation catalysis of perovskites relationships to bulk structure and composition. *Chem. Lett*., 16 (6) 41-65.